

Interplay of Physically Different Properties Leading to Challenges in Separating Lanthanide Cations – an *Ab Initio* Molecular Dynamics and Experimental Study

Kevin Leung,* Anastasia G. Ilgen, and Louise J. Criscenti

Sandia National Laboratories, MS 1415,

Albuquerque, NM 87185

*kleung@sandia.gov

(Dated: December 29, 2021)

Abstract

The lanthanide elements have well-documented similarities in their chemical behavior, which makes the valuable trivalent lanthanide cations (Ln^{3+}) particularly difficult to separate from each other in water. In this work, we apply *ab initio* molecular dynamics simulations to compare the free energies (ΔG_{ads}) associated with the adsorption of lanthanide cations to silica surfaces at a pH condition where SiO^- groups are present. The predicted ΔG_{ads} for lutetium (Lu^{3+}) and europium (Eu^{3+}) are similar within statistical uncertainties; this is in qualitative agreement with our batch adsorption measurements on silica. This finding is remarkable because the two cations exhibit hydration free energies (ΔG_{hyd}) that differ by >2 eV, different hydration numbers, and different hydrolysis behavior far from silica surfaces. We observe that the similarity in Lu^{3+} and Eu^{3+} ΔG_{ads} is the result of a delicate cancellation between the difference in Eu^{3+} and Lu^{3+} hydration (ΔG_{hyd}), and their difference in binding energies to silica. We propose that disrupting this cancellation at the two end points, either for adsorbed or completely desorbed lanthanides (e.g., *via* nanoconfinement or mixed solvents), will lead to effective Ln^{3+} separation.

I. INTRODUCTION

Lanthanide (Ln) series elements exhibit specific utility in green energy applications including lighting, wind turbines, electrified vehicles, and catalysis.¹ Improved mining and extraction techniques are needed to expand the inventory of these critical elements. Trivalent lanthanide cations (Ln^{3+}) naturally occur as mixtures. As such, separation of Ln^{3+} from each other is a technologically relevant and chemically challenging problem.²⁻⁵ Ln separation schemes are complicated and hazardous, and have to be adjusted depending on the composition of the Ln-containing ore. Ion-exchange separation of lanthanides has limited industrial use due to separation efficiencies of existing resins not yielding sufficient Ln^{3+} separation.⁶ Here we investigate what makes adsorption more or less selective, so in the future we can develop ion-exchange separation methods based on the fundamental science insight.

This separation problem has been addressed from several angles. Extensive basic science research has been conducted to elucidate the solvation properties of lanthanides in liquid water.⁷⁻¹² Further experimental^{2,4,5} and theoretical work¹³⁻¹⁵ has focused on separating Ln^{3+} from their mixtures using organic ligands. The results suggest that factors like pH, counter-ion effects, soft-hard ion concepts, and ligand rigidity are important.^{2,4,13-16} Additional studies have focused on the possibility of using silica and nanoporous silica materials (with and without functionalization of their surfaces) to adsorb¹⁷⁻¹⁹ and separate^{20,21} Ln^{3+} . This latter pathway has proven somewhat successful. At $\text{pH}\sim 4$, bare silica nanopores have been shown to selectively adsorb scandium,²¹ but selectivity among lanthanides appears limited. Ilgen has shown that, at $\text{pH}\sim 6$, smaller lanthanides cations are preferentially retained on nanoporous silica, depending on the nanopore size.²² At still higher pH values, lanthanides are less soluble and precipitate as hydroxides.²³ Improvement of such inorganic materials will likely enhance their Ln^{3+} selectivity, making them competitive with organic materials which are more costly, less durable, and less environmentally benign.

Further studies are needed to determine how separation mechanisms determined for organic ligands^{2,4,13-16} can be transferred to separation using inorganic materials. Computationally, molecular-level mechanistic studies have had difficulty determining lanthanide bonding to inorganic surfaces or the relevant adsorption/desorption free energies (ΔG_{ads}), in part because of a lack of classical force fields that accurately reflect the interaction between f -electron trivalent cations and water or silica surfaces.¹¹

In this work, we address the fundamental question of why different Ln^{3+} cations exhibit “chemically similar” adsorption equilibrium constants on silica within a specific pH range, despite their significantly different physical properties. For example, lanthanides are known to exhibit hydration free energies in liquid water (ΔG_{hyd}) that differ significantly, by >2 eV. Lutetium (Lu^{3+}) and europium (Eu^{3+}) are at the endpoint and midpoint of the $4f$ -electron block of the periodic table, respectively. Their ionic radii, differing by ~ 0.1 Å,⁷ are suf-

ficient to cause the Lu^{3+} ΔG_{hyd} to be more negative (*i.e.*, favorable) than that of Eu^{3+} by $\Delta\Delta G_{\text{hyd}}=-2.17$ eV.¹⁶ We will show that this difference far exceeds the relative adsorption free energy ($\Delta\Delta G_{\text{ads}}$). We will also demonstrate that the two Ln^{3+} exhibit different extent of hydrolysis reactions involving splitting of H_2O molecules in their inner spheres; such concerted hydrolysis/desorption behavior has been proposed and reported for other multivalent cations.^{18,24-27} As a result, Ln^{3+} hydration numbers (N_{hyd} , the numbers of H_2O molecules coordinated to different Ln^{3+}) can differ by two along parts of the desorption reaction pathway.

We apply the *ab initio* molecular dynamics (AIMD) method, based on Density Functional Theory (DFT), in conjunction with the potential-of-mean-force (PMF) method which effectively extends AIMD time scales to yield accurate free energies. We show that Eu^{3+} and Lu^{3+} exhibit very similar ΔG_{ads} . These predictions are supported by batch adsorption measurements on non-porous silica surfaces. The advantage of DFT is that it can be further applied to analyze different energy contributions. Our analysis leads us to conclude that Ln^{3+} are not very similar; instead, the cancellation of large energy terms leads to similar ΔG_{ads} that hinders separation. From this work, we propose that the key to successful Ln^{3+} separation technology resides in the disruption of this cancellation in either the adsorbed or desorbed regime.

This work involves significant computational challenges. The accuracy of DFT functionals and pseudopotentials used to treat Ln^{3+} needs to be addressed, and we will perform tests on one of the Ln^{3+} pseudopotential used in this work. However, there is an urgent need to address the accuracy of other modeling details as well, such the explicit treatment of both outer-shell solvating water molecules and the environment near interfaces. In implicit outer-shell solvation DFT calculations,^{8,16} the predicted ΔG_{hyd} exhibit variations that are on the order of a fraction of an eV. The discrepancies partly arise from the use of different DFT functionals or quantum chemistry methods, but variations in the implicit solvation methods used also likely play a role. In this work, we apply exclusively explicit hydration treatment via AIMD. We argue that such statistically mechanically rigorous research needs to take place in parallel with the development of more accurate DFT methods when dealing with Ln^{3+} in aqueous interfacial environments. AIMD calculations of ΔG_{ads} at water/mineral interfaces for trivalent lanthanide cations, or for any trivalent cations, remain rare and challenging because of the high charge density involved. Our work represents a key step in this direction.

II. METHOD

A. Experimental Details

Adsorption of Eu^{3+} and Lu^{3+} onto amorphous silica was quantified. We used commercially available fumed silica (Sigma Aldrich) with surface area of 192 ± 3 m^2 g^{-1} as reported

in our earlier work.²⁸ No background electrolyte or buffer were used. Milli-Q water with the resistivity of 18 M Ω -cm was used for all stock solutions and experiments. Lanthanide (Ln) stock solutions were prepared by diluting their nitrate salts Ln(NO₃)₃ in milli-Q water. Aqueous concentration was verified by inductively coupled plasma mass spectrometry (ICP-MS) analysis as described below.

Initially 50 \pm 1 mg of silica was weighted into each centrifuge vial, then 10 mL of Milli-Q H₂O was added, and samples were hydrated for a minimum of 2 hours. To begin the adsorption experiment, lanthanide stock solution was added, and the total volume of each sample was brought to 50 mL. The pH was measured after 2 hours of reaction and read at pH=5.0 \pm 0.3 for all samples. Then the samples were left on a shaker table for one-week (168 hours). Our preliminary kinetics runs showed that adsorption equilibrium is reached after 48 hours. The initial concentration of each lanthanide in the reactors was 0.1, 1, 10, 20, 30, and 50 μ M L⁻¹. The sample with 10 μ M L⁻¹ was made in triplicate to assess experimental error. All experiments were performed at ambient temperature (22 $^{\circ}$ C).

B. AIMD Computational Details

Finite temperature AIMD simulations apply the Perdew-Burke-Ernzerhof (PBE) functional,²⁹ the projector-augmented wave-based Vienna Atomic Simulation Package (VASP),^{30–33} a 400 eV energy cutoff, and Γ -point sampling of the Brillouin zone. A Nose thermostat maintains the temperature at a slightly elevated 400 K. A Born-Oppenheimer energy convergence criterion of 10⁻⁶ eV and a time step of 0.5 fs are enforced. These settings are similar to those in our previous ion desorption work.²⁵ The charge-neutral simulation cell has a Si₄₀O₈₈H₁₃³⁻ stoichiometry for the reconstructed β -cristobalite (001) slab, 123 H₂O molecules, and a Lu³⁺ or Eu³⁺ cation in an initially bidentate adsorbed configuration. All simulation cells have dimensions 14.32 \AA \times 14.32 \AA \times 26.0 \AA . They represent a 2^{1/2} \times 2^{1/2} expansion of simulation cells we previously applied.³⁴ The larger simulation cells are adopted because of the expectation that trivalent cations will experience stronger image-image interactions at the same cell size. The VASP lanthanide pseudopotential used are “Lu 23Dec2003” and “Eu 3 20Oct2008.” Lu³⁺ has no unpaired *f*-electrons and the Eu pseudopotential adopted (henceforth referred to as “Eu(A)”) subsumes its *f* electrons into the core; hence non-spin polarized DFT is applied for all AIMD simulations. Calculations using the Lu pseudopotential, with explicit 4*f* electrons, are expected to be more accurate than those using the Eu(A) pseudopotential, without explicit 4*f* electrons. Some static, spin-polarized DFT, DFT+U,³⁶ and HSE06^{37–39} calculations, using the “Eu 23Dec2003” (“Eu(B)”) pseudopotential with an explicit, partially filled *f*-shell, are conducted as spot checks (Sec. III D).

The number of H₂O molecules in the simulation cell is determined as follows. Classical

force field-based grand canonical Monte Carlo (GCMC)⁴⁰ simulations are first applied to determine the average number of water molecules filling the gap between the silica surfaces.³⁴ The SPC/E water model,⁴¹ a force field for silica based on OPLS,⁴² and generic force field parameters pertinent to Ln^{3+} are adopted for this purpose. Silica atoms and the adsorbed cation are frozen in DFT-optimized positions in GCMC calculations; only water molecules are inserted into or removed from the simulation cell. GCMC yields 7 H_2O molecules coordinated to the Ln^{3+} adsorbed to the surface. Switching to AIMD simulations and a Lu^{3+} cation reduces this to four after equilibration (Fig. S2a).

The AIMD calculations in this work omit dispersion corrections.⁴³ This enables comparison with our previous pK_a predictions which involve a similar computational protocol.³⁴ Adding dispersion is known to improve AIMD predictions of liquid water structure ($g(r)$) at $T=300$ K.⁴⁴ But it has yet to be demonstrated that this gives universally superior predictions at water/oxide interfaces.

In the presence of acid functional groups at water/material interfaces, the pH in the simulation cell should be pinned at the pK_a of functional groups, provided that (1) there is only one type of such groups; (2) a fraction of them are deprotonated; (3) their pK_a is lower than that of H_2O ; and (4) the surface groups do not interact with each other. Within the non-interacting assumption, the pH in our AIMD cells should be between 7.0 and 8.1 – the pK_a range previously predicted for this single type of SiOH on this surface.³⁴ In experimental samples with amorphous or crystalline silica, bimodal or trimodal pK_a distributions have been reported.^{45–47} It would have been more challenging to assign pK_a in AIMD simulation cells with multiple types of SiOH.

C. Potential-of-Mean-Force Details, Reaction Coordinates

The potential-of-mean-force profile is computed as $\Delta W(Z) = -k_{\text{B}}T \log P(Z)$ where $P(Z)$ is the probability that a Z value is recorded in the trajectory within a window, after making adjustments to rigorously remove the effect of umbrella sampling penalties. Here Z is the coordinate normal to the silica-water interface, $Z = z_{\text{Ln}} - z_{\text{Si}}$, Ln is the desorbing lanthanide cation, and Si is the Si atom close to the two O_{Si}^- groups initially coordinated to the Ln^{3+} . This coordinate is chosen to accommodate the strong electrostatic attraction between trivalent cations and surface silanol groups which can exhibit substantial bending motion. Harmonic penalties $A_o(Z - Z_i)^2$ are added to DFT energies in a series of windows with a progression of Z_i values, separated by 0.3 Å spanning the reaction paths. A_o is set at 2 eV/Å².

For Lu^{3+} , the initial configuration in the window has the cation coordinated to two SiO^- groups. Then AIMD is applied. Each subsequent window, with successively larger Z_i , and therefore greater extent of desorption, is initiated by taking a configuration near the end

of the trajectory from the previous window along the Z -coordinate. The first one or more picoseconds in each window is used for equilibration only; statistics are collected for up to 45 ps. Statistical uncertainties in $\Delta W(Z)$ are estimated by splitting the trajectory in each window into five, calculating the standard deviation in $\Delta W(Z)$ between the edge Z values in each window ($\Delta\Delta W(Z_i)$), and propagating the noise across windows assuming gaussian statistics. For Eu^{3+} simulations, each sampling window is initiated using an equilibrated configuration taken from the Lu^{3+} trajectory with the same Z_i value. This generally entails an increase in hydration number (N_{hyd}) by one compared to Lu^{3+} , and sometimes reduces the number of OH^- groups coordinated to the Eu^{3+} (N_{oh}). It typically takes 4-10 ps to equilibrate N_{hyd} for Eu^{3+} in each window. Trajectory lengths in different umbrella sampling window are listed in Table S1 in the ESI. The aggregate trajectory lengths used in all windows exceed 336 and 255 ps for Lu^{3+} and Eu^{3+} , respectively.

In the $Z_i=5.0 \text{ \AA}$ sampling window, the second of two $\text{O}_{\text{Si}}\text{-Ln}^{3+}$ ionic bond is being broken, forming two valleys in the free energy landscape with the absolute distance (not just z -coordinate) $R'=R_{\text{Ln-O}}$ centered around $R'=2.5 \text{ \AA}$ (with one $\text{O}_{\text{Si}}\text{-Ln}^{3+}$ bond) and 4.2 \AA (with zero, Sec. III B). These valleys are separated by a small free energy barrier. In sampling windows with $Z_i \ll 5.0 \text{ \AA}$, the $R' \sim 2.5 \text{ \AA}$ valley is strongly favored, while large Z_i strongly favors the $R' \sim 4.2 \text{ \AA}$ valley. As our reaction coordinate Z only constrains the vertical distance between Ln^{3+} and the designated Si atom, it does not yield a smooth transition between the two R' valleys in the handshake region near $R \sim 5.0 \text{ \AA}$ (Sec. III B).

To deal with this problem and generate a smooth $\Delta W(Z)$, a secondary umbrella sampling calculation is performed on reaction coordinate $R' = R_{\text{Ln-O}}$, as follows. (a) By trial and error, we locate the sampling window (or create a new sampling window) centered around $Z=Z_i$ where the $R_{\text{Ln-O}} \sim 2.5 \text{ \AA}$ and $R_{\text{Ln-O}} \sim 4.0 \text{ \AA}$ valleys are similar in free energy. This occurs at $Z_i=5.0 \text{ \AA}$ and 4.9 \AA for Eu and Lu, respectively. (b) Keeping the primary umbrella sampling A_o and Z_i parameters constant, we introduce a series of harmonic constraints C_o ($R'-R_i$)², with C_o chosen to be 1.5 or 2.0 eV/ \AA^2 and R_i separated by between 0.2 to 0.4 \AA . (c) Ideally, one would generate a 2-dimensional PMF plot with Z and R' . In reality, the relatively short AIMD simulations do not permit compiling accurate 2-D PMF statistics. Instead, we align the R' windows by integrating all Z contributions in a restricted range that feature in the two end-point R' sampling windows, so that there is overlapping statistics. The ranges chosen are $4.73 \text{ \AA} < Z < 4.83 \text{ \AA}$ for Lu^{3+} and $4.87 \text{ \AA} < Z < 4.97 \text{ \AA}$ for Eu^{3+} . (d) Integrating the $\Delta W(Z, R')$ over this narrow Z range generates a pre-factor F that describes the statistical weight of the two R' valleys. (e) If F is smaller than 1/15, we switch to larger Z_i and retry (a)-(d). If F is larger than 15, we decrease Z_i instead. As mentioned above, $Z_i=5.00 \text{ \AA}$ and 4.90 \AA are chosen for the Eu^{3+} and Lu^{3+} simulations via trial-and-error. (f) We add the probabilities $P(Z)$ from the two valleys, computed with $C_o=0$ (unconstrained in the R' coordinate), weighted by the factor F .

A less severe version of this problem was encountered in our previous calculations asso-

ciated with Cu^{2+} desorption.²⁵ The Cu^{2+} - $\text{O}(\text{SiO}^-)$ attraction is considerably weaker than the Ln^{3+} - $\text{O}(\text{SiO}^-)$ attraction, and a less elaborate procedure was devised to circumvent this issue.²⁵ The higher local charges associated with Ln^{3+} cations makes AIMD PMF desorption calculations more challenging.

Unlike Ref. 25, we do not use $Z = (z_{\text{O}} - z_{\text{M}})$ for reaction coordinate, where O is one of the O_{SiO}^- groups initially coordinated to the metal (“M”) cation. The attraction between Ln^{3+} and the O atom in a surface SiO^- group is stronger than in previous divalent cation calculations. As a result, using the previous $Z = (z_{\text{O}} - z_{\text{M}})$ coordinate can lead to the O atom being pushed into the silica interior while the Ln^{3+} cation remains on the surface, bonded to other surface silanol groups. Unlike Ref. 48, we do not use the distance $R = |\mathbf{R}_{\text{O}} - \mathbf{R}_{\text{M}}|$. This coordinate also allows the cation to roll along the surface on to different surface sites, instead of away from the surface into the bulk liquid. The water oxygen-cation coordination number N_{hyd} ⁴⁸ is not used for our purpose; it does not distinguish possible outer-sphere ($\text{Ln}^{3+}/\text{H}_2\text{O}/\text{SiO}^-$) complexes, where Ln^{3+} and SiO^- are 3.5-4.5 Å apart, from Ln^{3+} completely dissociated from SiO^- .⁴⁹ Furthermore, for Lu^{3+} , N_{hyd} does not increase monotonically as the cation desorbs.

Another, weaker harmonic potential of the form $B_o[(\delta x - x_o)^2 + (\delta y - y_o)^2]$ constrains the Ln-O distances in the lateral directions. Here $B_o=0.025$ eV, $\delta x=x_{\text{Ln}} - x_o$, x_o is the equilibrium value of δx computed in completely unconstrained AIMD trajectories, and δy and y_o are defined in analogous ways.

$\Delta W(Z)$ is effectively the constrained free energy at a Z value; it does not include the standard state reference associated with aqueous solutions. To obtain the adsorption free energy (ΔG_{ads}) from $\Delta W(Z)$, we integrate configuration space in three dimensions, and account for the entropic contribution from a standard state 1.0 M ideal concentration solution:⁵⁰

$$\Delta G_{\text{ads}}/k_{\text{B}}T = -\log\left\{\int_{\Omega} d\Omega \exp[-\Delta W(Z)/k_{\text{B}}T]/(V_o)\right\}. \quad (1)$$

Here V_o is the volume associated with 1.0 M aqueous solution (1662 \AA^3) and $T=300$ K is assumed. (“Standard state” refers to $[\text{Ln}^{3+}]=1.0$ M; no attempt is made to adjust the pH in Eq. 1.) The volume element Ω spans the configuration space where Ln^{3+} is “bonded” to the SiO^- group. A limiting bonding distance of 3.20 Å is assumed. At this separation the pair correlation functions between transition metal ions and water oxygen sites exhibit their first correlation minima (Fig. S1 in the ESI). The angular distribution is also involved in the integral. To our knowledge, Ω has not been standardized for PMF calculations at interfaces.^{48,49,51} Here we approximate it as a cylinder with a radius $R=0.5$ Å. Electrostatic corrections associated with image dipoles are added to the PMF predictions by creating a lattice model with screened coulomb interactions.²⁵

We do not apply the metadynamics method, based on non-equilibrium trajectories, to compute the PMF.⁵² The umbrella sampling approach used herein permits us to run trajectories of variable lengths not determined ahead of time. We examine statistical uncertainties

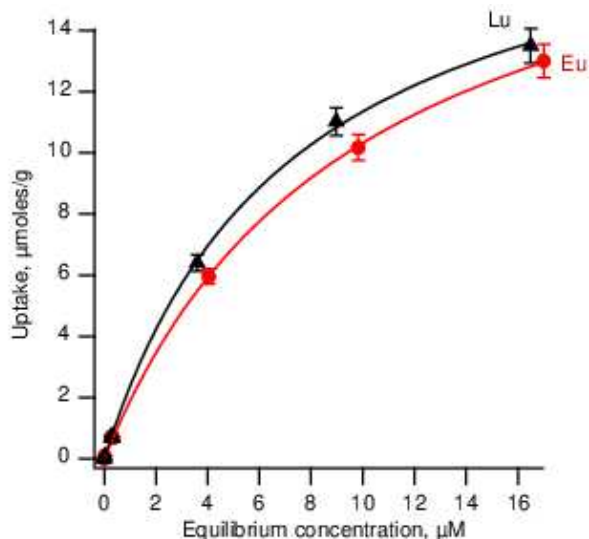


FIG. 1: Uptake of Eu^{3+} and Lu^{3+} on amorphous silica SiO_2 . Points = data, lines = fits for Langmuir isotherm equation. Cumulative experimental error shown as error-bars was 4.2%.

in each window to make sure there is no large, systematic drift in $\Delta W(R)$ in each AIMD trajectory.

III. RESULTS AND DISCUSSIONS

A. Batch Adsorption

First we discuss batch adsorption results on amorphous silica surfaces that motivated this work (Fig. 1). The experiments were performed on silica surfaces with ~ 2 SiOH groups per nm^2 of surface, as discussed in our earlier publication.²⁸ The lanthanide adsorption data was fit using the Langmuir isotherm model. Based on the fitting, the maximum adsorption coverage for Eu^{3+} was estimated at $20.4 \mu\text{moles/g}$, and the Langmuir constant K_L was 0.102 L/g . For Lu^{3+} the maximum adsorption was estimated at $19.6 \mu\text{moles/g}$, and K_L at 0.138 L/g . The overall affinity at pH 5.0 for Lu^{3+} and Eu^{3+} was similar, with Lu^{3+} being slightly more favorable. This suggests that the experimental ΔG_{ads} for Eu^{3+} and Lu^{3+} are very similar.

B. Potential-of-Mean-Force

Next we turn to AIMD modeling. Fig. 2a depicts the charge-neutral simulation cell containing 123 H_2O molecules and a partially deprotonated, surface-reconstructed β -cristobalite slab; Lu^{3+} is coordinated to two SiO^- groups on one surface. Fig. 2b-e depict Lu^{3+} con-

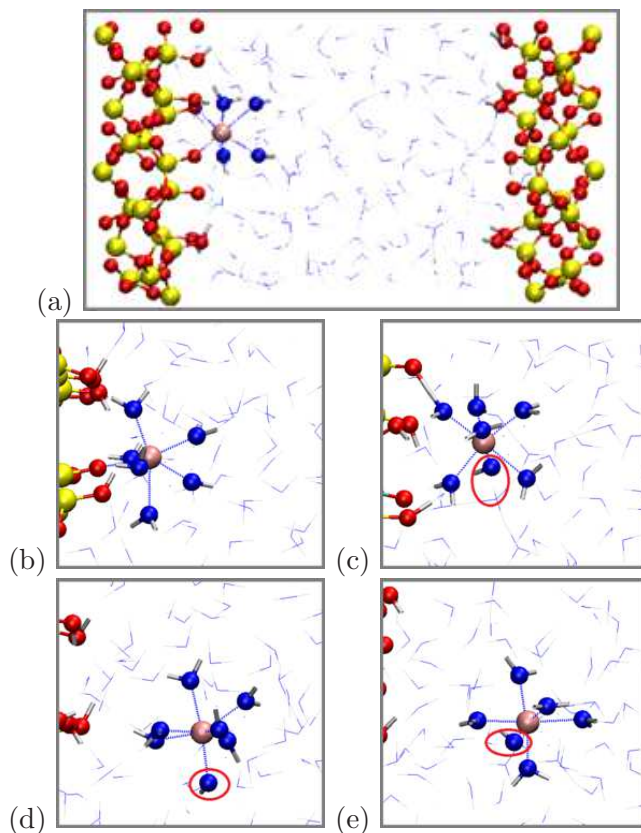


FIG. 2: (a) The $14.3 \times 14.3 \times 26 \text{ \AA}^3$ simulation cell with adsorbed Lu^{3+} complex coordinated to two SiO^- groups. The reaction coordinate Z is along the z direction (left-to-right). (b)-(c) Z centered at $Z_i=4.9 \text{ \AA}$, with Lu^{3+} bound to two or one SiO^- groups. (d) $Z_i=7.4 \text{ \AA}$. (e) $Z_i=8.0 \text{ \AA}$. Z_i is the center of the constrained window. Si, O, O (water), H, and Lu are depicted in yellow, red, blue, white, and pink. As some protons in H_2O are obscured, the true OH^- species are circled in red.

figurations in different PMF sampling windows as the cation desorbs. The SiOH surface density is $4.0/\text{nm}^2$, and unlike in the experiments there are no counter-ions. Nevertheless, qualitative comparisons can be made.

Fig. 3a compares $\Delta W(Z)$ for Lu^{3+} and Eu^{3+} . The shapes of $\Delta W(Z)$ at small Z are similar, suggesting similar energetics in the neighborhood of the optimal adsorption configuration. As desorption proceeds and Z approaches $Z \sim 5 \text{ \AA}$, a cross-over to a quasi-plateau region is observed. The Eu^{3+} potential-of-mean-force exhibits a slight repulsive behavior ($\Delta W(Z) > 0$) near $Z=5 \text{ \AA}$. This is likely related to overscreening behavior associated with multivalent electrolytes.⁵³ In contrast, due to hydrolysis in its hydration shell (see below), the more weakly charged, hydrolyzed $\text{Lu}^{3+}(\text{OH}^-)_n$ complexes have a lower net charge and a monotonic $\Delta W(Z)$. Our AIMD simulations are not ideally suited to investigating overscreening effects due to the lack of counter-ions. However, our future classical force field MD simulations will reconsider possible overscreening. Neither cation exhibits a local minimum

associated with outer sphere solvation; local minima may have been helpful in engineering preferential adsorption motifs.

Integrating $\Delta W(Z)$ yields $\Delta G_{\text{ads}}=-0.79\pm 0.04$ eV and -0.84 ± 0.03 eV, assuming standard states for Lu^{3+} and Eu^{3+} . The uncertainties reflect one standard deviation. Not included in Fig. 3a are electrostatic corrections. As the Ln^{3+} desorbs, a significant dipole moment is created in the simulation cell, leading to image-image repulsions in the lateral directions. Using corrections based on lattice-models with dielectric screening,²⁵ the magnitudes of ΔG_{ads} are reduced by 0.01 and 0.09 eV for Lu^{3+} and Eu^{3+} , respectively. These corrections change the preferred adsorption from Eu^{3+} over Lu^{3+} to Lu^{3+} over Eu^{3+} by 0.03 eV, because the $\text{Lu}^{3+}(\text{OH}^-)_n$ complex incurs less correction. The computed ΔG_{ads} are larger in magnitude than our AIMD predictions of divalent metal cations on mineral surfaces, which range from -0.38 to -0.71 eV.²⁵ Our predicted Ln^{3+} ΔG_{ads} are more negative than those measured for some trivalent cations on silica surfaces,¹⁸ likely because of the higher effective pH in our simulations, our absence of counter-ions, and possible differences in SiOH spatial distributions between our model and the experiment samples. The measurements in Ref. 18 are conducted at pH=4 while the pH in our simulation cell is estimated to be ~ 7.5 . A 3.5 unit increase in pH translates into a maximum of $2\times 3.5\times 0.059$ eV=0.41 eV increase in Ln^{3+} binding free energy. This estimate assumes that the increase in pH reduces the free energy needed to deprotonate two neighboring SiOH groups, which then bind to the Ln^{3+} . It is much more difficult to quantify the dependence of ΔG_{ads} on surface structure details, such as the distance between the two SiO^- groups coordinated to the adsorbed Ln^{3+} , without explicit AIMD/PMF simulations of the modified structure. We plan to pursue AIMD simulations of monodentate Ln^{3+} on model silica surfaces in the future.

As discussed in Sec. II C, around $Z_i=5.0$ Å, a secondary PMF calculation, with another reaction coordinate R' , which is the true distance between the Ln^{3+} and a flagged O atom (not just its z -component), is needed to augment our results. Fig. 4a shows that the Eu^{3+} $\Delta W(Z)$ in the $Z<5.0$ Å and $Z>5.0$ Å, windows (green and blue lines) have different slopes. Combining these curves would yield a sharp kink in $\Delta W(Z)$. A similar kink would have occurred in the Lu^{3+} $\Delta W(Z)$ (Fig. 4c). These kinks signal the inability of AIMD/PMF simulations to reversibly sample two free energy valleys separated by small barriers. Fig. 2b-c show that these valleys are in fact associated with Lu^{3+} coordinated to one and zero SiO^- groups, respectively; the local minima are separated by Lu^{3+} displacement parallel to the silica surface. In terms of the secondary coordinate, R' jumps from 2.5 to 4.2 Å between these valleys. Our secondary PMF $\Delta W'(R')$ estimates the free energy differences between these two valleys (Sec. II C) and largely smooths over the kink in $\Delta W(Z)$. The barrier between the valleys are 0.2 to 0.25 eV (Fig. 4b,d), which are small but would have required much longer AIMD trajectories to sample adequately without the secondary PMF. While this approach involves approximations (Sec. II C), the uncertainty in $\Delta\Delta G_{\text{ads}}$ is lessened

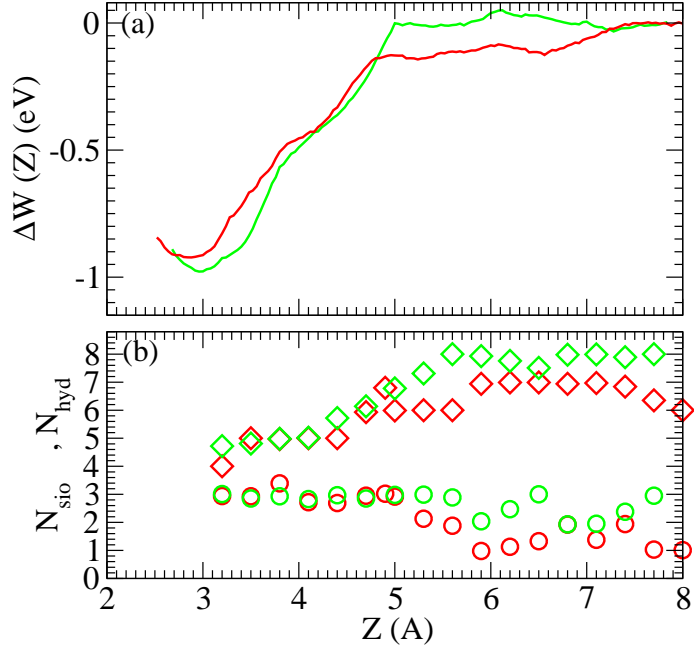


FIG. 3: (a) Free energy profile along desorption reaction coordinate Z . Red and green are for Lu^{3+} and Eu^{3+} , respectively. (b) Average number of SiO^- groups (N_{seo} , circles) in the simulation cell, and the Ln^{3+} hydration number (N_{hyd} , diamonds). The number of hydrolyzed H_2O molecules coordinated to the Ln^{3+} is $N_{\text{oh}}=(3-N_{\text{seo}})$ on average.

due to the expected cancellation of errors between Lu^{3+} and Eu^{3+} .

C. Surprisingly Large Energy Difference in Adsorbed States

The predicted preferential Lu^{3+} adsorption is qualitatively consistent with our batch adsorption measurements (Fig. 1). The difference between the Lu^{3+} and Eu^{3+} ΔG_{ads} is small, comparable to the statistical uncertainty. However, this small $\Delta\Delta G_{\text{ads}}=-0.03$ eV, is surprising from an energetic standpoint – despite the much-quoted lanthanide “chemical similarity.” As mentioned above, Lu^{3+} exhibits ΔG_{hyd} which is more favorable (negative) than the Eu^{3+} value by -2.17 eV.¹⁶ This represents the desorption end point behavior. For the two ΔG_{ads} to be similar, there must be a similarly large energetic difference at the adsorbed end point where Lu^{3+} and Eu^{3+} are in contact with silica. In other words, chemical similarity in fact derives from a cancellation of large (relative) energy terms.

To examine this hypothesis, we approximate the energy difference ($\Delta\Delta E_{\text{ads}}(\text{dry})$) in the adsorbed state by omitting most water molecules. We optimize configurations with a Lu^{3+} or Eu^{3+} cation at the binding site coordinated to two SiO^- groups at $T=0$ K (Fig. 5a-b). Only one H_2O molecule is included in the simulation cell. Maximally localized Wannier

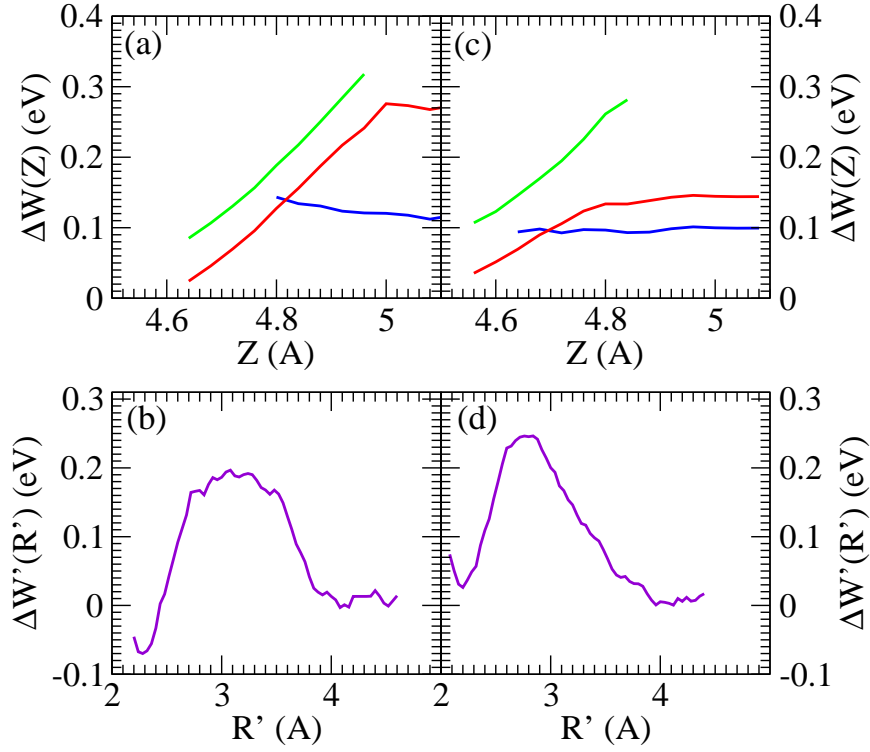


FIG. 4: Panels (a)-(b) and (c)-(d) refer to $\Delta W(Z)$ for Eu^{3+} and Lu^{3+} , with $Z_i=5.0 \text{ \AA}$ or $Z_i=4.9 \text{ \AA}$, respectively. Green and blue are unnormalized $\Delta W(Z)$ segments in the two R' free energy valleys with the same Z_i constraint; they correspond to Ln^{3+} coordinated to one or zero SiO^- . Red depicts a weighted average of the two, based on secondary umbrella sampling. (b) and (d): potential-of-mean force along a secondary reaction coordinate R' ($\Delta W'(R')$), with R' being one of the O-Ln distances. See text.

function analysis⁵⁴ confirms that, in these charge-neutral simulation cells with significant vacuum regions, both lanthanides remain trivalent cations. The net energy of the Lu^{3+} simulation cell is lower than that of Eu^{3+} by $\Delta\Delta E_{\text{ads}}(\text{dry})=-1.68 \text{ eV}$ after subtracting the respective gas phase, bare ion energies. This difference is indeed similar to the reported -2.17 eV difference in ΔG_{hyd} .¹⁵ Note that we cannot report accurate absolute binding energies between Ln^{3+} and negatively charged silica because of the difficulty in correcting the energies of slabs with net charges.

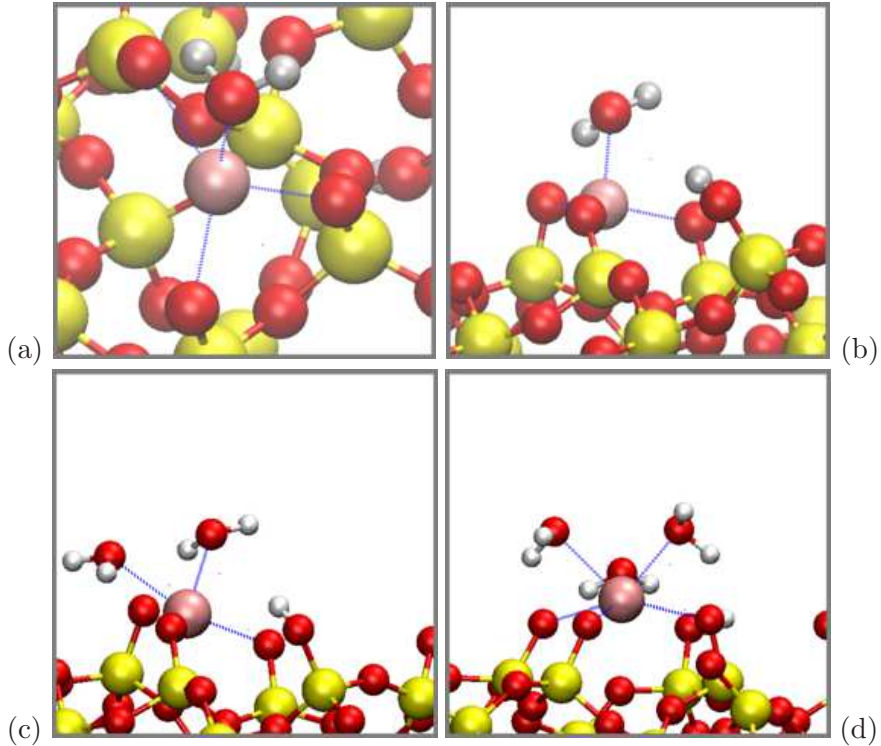


FIG. 5: (a)-(b) Top and side views of optimized Lu^{3+} adsorption configuration on silica surface, at $T=0$ K and coordinated to one H_2O molecule. (c)-(d) Similar to (b) but with two and three H_2O coordinated to Eu^{3+} , respectively.

D. Justification for Using the Eu(A) Pseudopotential

The systems depicted in Fig. 5 also represent convenient platforms to examine the validity of the Eu(A) pseudopotential used, which omits f -electrons. It is tempting to assume that Eu(B), which includes f -electrons and requires the spin-polarized DFT method (Sec. II B), would be more accurate. Our attempts at using Eu(B) in DFT/PBE-based AIMD simulations, however, result in occasional failures in the self-consistent field procedure when performing convergence of the Kohn-Sham densities and the Slater determinant orbitals. The likely reason is an unphysical charge transfer from silica to the Eu^{3+} when using this pseudopotential during AIMD. This is likely a failure of the PBE functional, which is known to predict unphysical electron delocalization in f -electron systems like CeO_2 .^{55,56} To deal with this problem, the DFT+U method³⁶ has often been applied as a remedy,⁵⁷ as have hybrid DFT functionals like HSE06.³⁷⁻³⁹

Here we compute the Eu(B)-predicted binding energies of a Eu^{3+} relative to Lu^{3+} to the $\text{Si}_{40}\text{O}_{88}\text{H}_{13}^{3-}$ slab (Fig. 5b) in vacuum, using the Eu(A) value as a reference. If both Eu pseudopotentials are equally accurate within the DFT/PBE framework, the energy difference ($\Delta\Delta E$) between them should be zero. Instead, we find that the Eu(B) result is favored by

$\Delta\Delta E = -0.70$ eV over Eu(A). When two or three H₂O are included (Fig. 5c-d), $\Delta\Delta E = -0.51$ eV and -0.48 eV, respectively.

Eu(B) gives consistently lower energies. We argue that the significantly more negative $\Delta\Delta E$ is consistent with unphysical hybridization between silica and Eu(B) $4f$ -orbitals, and/or possible electron transfer from silica to Eu³⁺. Note that the extent of charge-transfer is non-trivial to quantify; Wannier function analysis is challenging when using Eu(B), because the partially-filled f shell gives “metallic” behavior. To support our argument, we turn to a rotationally invariant DFT+U approach³⁶ with $U-J=4.5$ eV. We find that $\Delta\Delta E = -0.13$ eV, -0.11 eV, and -0.04 eV with 1-3 H₂O in the simulation cell. Therefore the Eu(A) pseudopotential yields predictions very similar to Eu(B) which has f -electrons – as long as the more reliable⁵⁷ DFT+U augmentation is applied to f -electrons in the latter case. Eu(A) does not have $4f$ electrons and DFT+U is inapplicable there, while Lu has a full $4f$ shell and DFT+U is not expected to yield results significantly different from PBE predictions. We also note that the Eu(A) and Eu(B) pseudopotentials have been shown to yield similar structural properties when the latter is used in conjunction with DFT+U augmentation.⁵⁸

Although applying DFT+U alongside the Eu(B) pseudopotential gives better agreement with Eu(A), the results slightly vary with the value of $(U-J)$. Sec. S3 in the SEI reports that changing $(U-J)$ from 4.5 eV to 6.5 eV for the one-water (Fig. 5a-b) configuration changes $\Delta\Delta E$ from -0.13 eV to 0.05 eV. Although this variation is only 0.18 eV, it is significant compared with the $\Delta\Delta G_{\text{ads}} = 0.03$ eV difference computed in AIMD simulations. To lessen this ambiguity, we also apply the HSE06 functional to both Lu³⁺ and Eu³⁺ bound to silica surfaces. The HSE06 $\Delta\Delta E$ for the Fig. 5a-b configuration is found to be -0.06 eV, which is close to zero. We argue that the Eu(A) pseudopotential, used in the majority of this paper, is an approximate way to implement HSE06, or DFT+U with $U-J=4.5$ eV, on the Eu pseudopotential with f -electrons. It should in fact give more physical results than Eu(B) when the latter is applied with PBE only. From these state calculations, we estimate that the systematic uncertainty associated with using the Eu(A) pseudopotential in our AIMD $\Delta\Delta G_{\text{ads}}$ calculations is between ~ 0.06 and 0.13 eV.

E. Hydrolysis and Hydration Behavior

In the rest of this paper we analyze the differences in Lu³⁺ and Eu³⁺ hydrolysis and hydration properties in an attempt to identify factors that promote preferential Ln³⁺ adsorption and separation. As noted above, initially Lu³⁺ is coordinated to two SiO⁻ groups and 4 H₂O molecules (Fig. 2a). Bidentate adsorption is consistent with dihydroxyl Yb³⁺ coordination at low Yb³⁺ coverage known from previous analysis.⁵⁹ In the cross-over region ($Z \sim 4.9$ Å), there is an equilibrium between two states, with Lu³⁺ coordinated to one (Fig. 2b) and zero SiO⁻ (Fig. 2c) group. Hydrolysis only occurs above $Z \sim 5$ Å; it arises

from the transfer of proton(s) from H₂O molecule(s) coordinated to the Lu³⁺, to the silica surface *via* the Grotthuss mechanism. When the desorption is almost complete (Fig. 2d-e), Lu³⁺ forms a Lu³⁺(H₂O)₆(OH⁻), a Lu³⁺(H₂O)₅(OH⁻)₂, or a Lu³⁺(H₂O)₄(OH⁻)₂ complex.

Eu³⁺ configurations (not shown) are qualitatively similar. Two main differences are that Eu³⁺ exhibits less tendency towards hydrolysis than Lu³⁺, and has larger hydration numbers (N_{hyd}) throughout the entire Z range. First we focus on hydrolysis. Fig. 3b reports $N_{\text{σιο}}$ as Z varies. $N_{\text{σιο}}$ counts the number of deprotonated Si-OH surface groups with a 1.25 Å O-H cutoff distance in each sampling window each centered at $Z=Z_i$. $N_{\text{σιο}}$ plus N_{oh} (the number of hydrolysis events or number of OH⁻ coordinated to Ln³⁺) should add to 3.0 on average. When $Z>5$ Å, the average $N_{\text{σιο}}$ is larger in Eu³⁺ simulation cells compared to Lu³⁺, meaning Eu³⁺ induces less hydrolysis. Like Lu³⁺, the onset in SiO⁻ protonation state change is correlated with the onset of the Eu³⁺ $\Delta W(Z)$ plateau.

Based on the above analysis, it is surprising that a substantial cancellation in energetics occurs for these two cations during desorption. Although the Lu³⁺/SiO₂ (Fig. 5a) and the Eu³⁺/SiO₂ binding configurations are similar (the latter is not shown), Lu³⁺ is coordinated to OH⁻ while Eu³⁺ is coordinated only to H₂O far from the surface. We conjecture that a substantial energy cancellation may arise from the fact that the pK_{a1} for hydrolysis is not far from the simulation cell pH condition, so there is little change in $\Delta\Delta G_{\text{hyd}}$ regardless of whether hydrolysis occurs. Indeed, beyond $Z=5$ Å, $\Delta W(Z)$ only changes by ~ 0.1 eV in the $\Delta W(R)$ for both cations. Hence we argue that hydrolysis does not strongly affect the predicted ΔG_{ads} for either Eu³⁺ or Lu³⁺. This is unlike the case of Cu²⁺.²⁵ We propose that, if a *local* pH significantly higher than the Ln³⁺(H₂O) _{n} pK_{a1} can be maintained, this crucial cancellation can be disrupted without causing Ln(OH)₃ precipitation, leading to more selective Ln³⁺ adsorption on silica surfaces.

Next we examine how differences in hydration numbers can affect $\Delta\Delta G_{\text{ads}}$. Fig. 3b also reports N_{hyd} , which is the number of H₂O or OH⁻ oxygen atoms within 3.2 Å of Ln³⁺. It does not count coordination to SiO⁻ groups. Eu³⁺ exhibits hydration numbers which exceed those of Lu³⁺ by about 1-2 in the entire Z range, i.e., $\Delta N_{\text{hyd}}\sim 1-2$. Note that Ln³⁺ hydration numbers in liquid water are measurable in X-ray and neutron scattering experiments, and much computational effort has been devoted to reproducing those values. We do not observe Lu³⁺(H₂O)₈ and Eu³⁺(H₂O)₉ complexes which have been predicted in quantum chemistry or molecular dynamics simulations.⁷⁻¹⁰ One reason is the Lu³⁺ inner sphere hydrolysis behavior discussed above, which has not been accounted for in previous modeling work.¹⁶ Indeed, metal cations coordinated to one or more OH⁻ have been known to yield reduced coordination numbers.^{25,60} Another reason may be that the explicit treatment of the second hydration shell in AIMD simulations changes the first shell hydration number computed using an implicit solvent approximation in the literature. Finally, different DFT functionals can yield N_{hyd} which are slightly different from each other and from experiments.⁶¹ The free energy difference associated with N_{hyd} values that differ by one is generally on the order

of $k_B T = 0.025$ eV, which is small on our $\Delta W(Z)$ energy scale. We propose that surface constraints or functional groups that increase ΔN_{hyd} to 2 or higher may be needed to aid selective adsorption.

F. Sampling Dynamics

For completeness, we briefly discuss dynamics. N_{hyd} and N_{oh} for Lu^{3+} are depicted as functions of time in selected sampling windows in Fig. 6. (The complete set is given in the ESI.) We have plotted N_{oh} instead of $N_{\text{σιο}}$ here because, at certain times, a H^+ may be in transit from the hydration shell of the desorbed Ln^{3+} to the silica surface; therefore $N_{\text{oh}}(t)$ is more descriptive than $N_{\text{σιο}}$ which equals $(3 - N_{\text{oh}})$ only on average. At $Z > 5$ Å, the average N_{oh} is not monotonic as Z varies, and there are picosecond time scale proton exchanges between the Lu^{3+} inner hydration shell and the silica surface not accompanied by significant changes in $\Delta W(Z)$ (Fig. 6). We never observe Si-OH groups from the opposite surface of the silica slab being involved in acid-base reactions.

Fluctuations of N_{hyd} for trivalent cations can take long times at room temperature. Fortunately, our sampling efficiency is improved by a slightly elevated temperature of 400 K. The fast proton transfer dynamics and the large driving force guiding N_{hyd} evolution as Z varies also help inner sphere equilibration. As a test, we have confirmed that, after removing the umbrella sampling constraint for Lu^{3+} at $Z_i = 3.5$ Å, N_{hyd} spontaneously relaxes from 5 to its equilibrium value of 4 (Fig. 3b) within 5 ps as the Lu^{3+} relaxes to its adsorbed configuration. See also the ESI for discussions of the special case of the N_{hyd} in one Lu^{3+} window. However, our simulation time scales would have been insufficient to deal with the presence of anions, which diffuse through water much more slowly than H^+ . This is the main reason we have not included explicit counter anions in our AIMD simulations, despite the fact that our batch adsorption experiments include NO_3^- .

IV. CONCLUSION

In summary, using AIMD/PMF calculations, we predict a slight, 0.03 ± 0.05 eV preferential adsorption of Lu^{3+} over the lighter, larger Eu^{3+} on model silica surface with deprotonated silanol groups at its interface. This finding is in qualitative agreement with our batch adsorption work. The 0.03 eV difference should be considered qualitative because of differences between the experimental and computational systems, which include silica surface details; pH; the presence/absence of NO_3^- counter-ions; multiple surface binding sites; and possible Ln^{3+} dimerization. We also note that our Lu^{3+} and Eu^{3+} calculations utilize Lu and Eu pseudopotentials with and without explicit $4f$ -electrons, respectively. As a result, the Lu^{3+} predictions are likely more accurate than the Eu^{3+} predictions. It is challenging to model

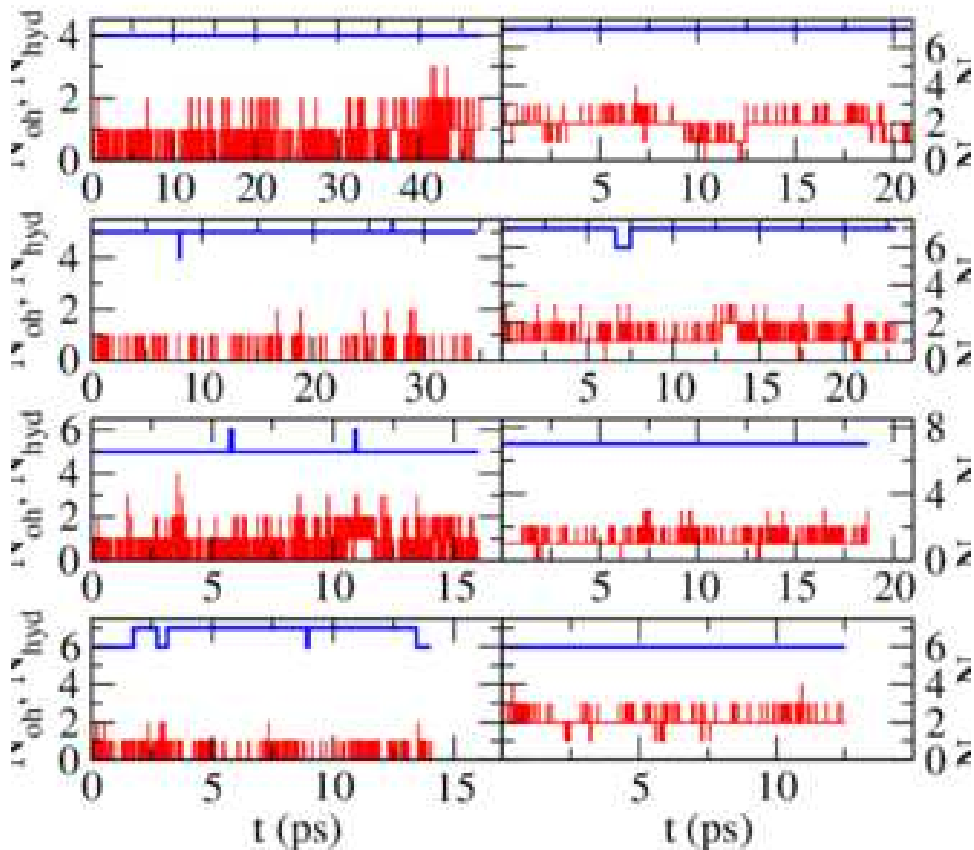


FIG. 6: N_{oh} (red) and N_{hyd} (blue) as functions of time (ps) in several Lu^{3+} sampling windows. From up to down, left column and then right: unconstrained AIMD, $Z_i=3.50 \text{ \AA}$, 3.80 \AA , 4.40 \AA , 5.60 \AA , 6.80 \AA , 7.40 \AA , and 8.00 \AA , respectively.

Ln^{3+} in aqueous media, both because of DFT functional accuracy issues and because of the statistical mechanical details that need to be implemented to obtain accurate free energy changes associated with highly charged trivalent cations which can desorb in conjunction with hydrolysis reactions. In that sense, our pioneering AIMD simulations pave the way for future examination of these details *via* systematic variation of the model surface. We explicitly address the role of concerted proton motion, and give quantitative desorption free energy predictions for trivalent lanthanide cation adsorption on mineral surfaces. Our predictions provide guidance to molecular dynamics simulations that apply classical force fields.

AIMD simulations are first-principles in nature, and are generally more accurate than force field-based MD. They are computationally costly; the necessarily limited trajectory

lengths lead to unavoidable statistical uncertainties. A ~ 10 -fold preference for Lu^{3+} over Eu^{3+} at $T=300$ K, measured under conditions slightly different from this work,²² translates into a -0.059 eV difference in ΔG_{ads} , which is almost within AIMD noise level. Instead of resolving small ΔG_{ads} differences, AIMD is most valuable at providing mechanistic insights. Thus it is more significant that the similarity of the Lu^{3+} and Eu^{3+} desorption free energies is found to arise from a cancellation between their relative adsorption energies to deprotonated silica surface ($\Delta\Delta E_{\text{ads}}(\text{dry})$), and their relative hydration free energies in liquid water ($\Delta\Delta G_{\text{hyd}}$). Although the cations exhibit substantial differences in hydration and hydrolysis properties, the cancellation leads to very similar ΔG_{ads} . To disrupt this cancellation of energy differences, enhance Ln^{3+} selectivity, and aid separation, we propose that modification of the silica surface to change the local pH or hydration environment, would be valuable. Another approach suggested by our analysis is to modify ΔG_{hyd} in the desorbed state, *e.g.*, by using a mixed solvent, or *via* nanoconfinement.²²

Conflicts of Interest

Nothing to declare.

Acknowledgement

We thank Jacob Harvey for his recommendation about Eu pseudopotentials and other suggestions, and Jacquilyn Weeks for assistance with the manuscript. This work is based on materials support by the U.S. DOE Office of Basic Energy Sciences, Division of Chemical Sciences, Geosciences, and Biosciences under Field Work Proposal Number 21-015452. Sandia National Laboratories is a multi-mission laboratory managed and operated by National Technology and Engineering Solutions of Sandia, LLC, a wholly owned subsidiary of Honeywell International, Inc., for the U.S. Department of Energy’s National Nuclear Security Administration under contract DE-NA0003525. This paper describes objective technical results and analysis. Any subjective views or opinions that might be expressed in the document do not necessarily represent the views of the U.S. Department of Energy or the United States Government.

-
- ¹ J.H.L. Voncken, *The Rare Earth Elements: An Introduction*. (Springer, 2015).
- ² G. Ferru, D.G. Rodrigues, L. Berthon, O. Diat, P. Bauduin and P. Guilbaud, *Angewandte Chem. Int. Ed.* 2014, **53**, 5346-5350.
- ³ I. Lehman-Andino, J. Su, K.E. Papathanasiou, T.M. Eaton, J.W. Jian, D. Dan, T.E. Albrecht-Schmitt, C.J. Dares, E.R. Batista, P. Yang, J.K. Gibson, K. Kavallieratos, *Chem. Commun.* 2019, **55**, 2441-2444.
- ⁴ F.W. Lewis, L.M. Harwood, M.J. Hudson, A. Geist, V.N. Kozhevnikov, P. Distler, J. John, *Chem. Sci.* 2015, **6**, 4812-4821.
- ⁵ H. Zhang, R.G. McDowell, L.R. Martin, Y. Qiang, *ACS Appl. Mater. Interfaces* 2016, **8**, 9523-9531.
- ⁶ N. Krishnamurthy, C.K. Gupta, *Extractive Metallurgy of Rare Earths*. (2016, CRC press)
- ⁷ P. D'Angelo, A. Zitolo, V. Migliorati, G. Chillemi, M. Duvail, P. Vitorge, S. Abadie and R. Spezia, *Inorg. Chem.* 2011, **50**, 4572-4579.
- ⁸ P. D'Angelo and R. Spezia, *Eur. J. Chem.* 2012 **18**, 11162-11178.
- ⁹ V. Migliorati, A. Serva, F.M. Terenzio and P. D'Angelo, *Inorg. Chem.* 2017, **56**, 6214-6224.
- ¹⁰ I. Persson, P. D'Angelo, S. De Panfilis, M. Sandström and L. Eriksson, *Chem. Eur. J.* 2008, **14**, 3056-3066.
- ¹¹ J. Kuta, M.C.F. Wander, Z. Wang, S. Jiang, N.A. Wall, A.E. Clark, A.E. *J. Phys. Chem. C* 2011, **115**, 21120-21127.
- ¹² D. Yu, R. Du, J.-C. Xiao, S. Xu, C. Rong and S. Liu, *J. Phys. Chem. A* 2018, **122**, 700-707.
- ¹³ A.S. Ivanov and V.S. Bryantsev, *Eur. J. Inorg. Chem.* 2016, 3474-3479
- ¹⁴ M.R. Healy, A.S. Ivanov, Y. Karslyan, V.S. Bryantsev, B.A. Moyer and S. Jansone-Popova, *Chem. Eur. J.* 2019, **25**, 6326-6331.
- ¹⁵ B. Sadhu and M. Dolg, *Inorg. Chem.* 2019, **58**, 9738-9748.
- ¹⁶ J. Ciupka, X. Cao-Dolg, J. Wiebke and M. Dolg, *Phys. Chem. Chem. Phys.* 2010, **12**, 13215-13223.
- ¹⁷ D.S. Jordan, J.N. Malin and F.M. Geiger, *Environ. Sci. Technol.* 2010, **44**, 5862-5867.
- ¹⁸ D.S. Jordan, S.A. Saslow and F.M. Geiger, *J. Phys. Chem. A* 2011, **115**, 14438-14445.
- ¹⁹ D. Garcia, J. Lützenkirchen, V. Petrov, M. Siebentritt, D. Schild, G. Lefevre, T. Rabung, M. Altmaier, S. Kalmykov, L. Duro and H. Geckeis, *Coll. Surfaces A* 2019, **578**, 123610.
- ²⁰ Y. Hu, E. Drouin, D. Lariviere, F. Kleitz and F.-G. Fontaine, *ACS Appl. Mater. Interfaces* 2017, **9**, 38584-38593.
- ²¹ S. Giret, Y. Hu, N. Masoumifard, J.-F. Boulanger, E. Juere, F. Kleitz and D. Lariviere, *ACS Appl. Mater. Interfaces*, 2018, **10**, 448-457.
- ²² A.G. Ilgen A.G. Non-provisional patent application "Systems and Methods for Separating Rare

- Earth Elements Using Mesoporous Materials.” Filed on 3/11/2020.
- ²³ W. Zhang and R.Q. Honaker, *Int. J. Coal Geology* 2018, **195**, 189-199.
- ²⁴ N. Marmier, J. Dumonceau and F. Fromage, *J. Contaminant Hydrology* 1997, *26*, 159-167.
- ²⁵ K. Leung, L.J. Criscenti, A.W. Knight, A.G. Ilgen, T.A. Ho, and J.A. Greathouse, *J. Phys. Chem. Lett.* 2018, **9**, 5379-5385.
- ²⁶ V. Alexandrov and K.M. Rosso, *Phys. Chem. Chem. Phys.* 2015, **17**, 14518-14531.
- ²⁷ Proton transfer-coupled processes, like redox reactions, have been prominent in physical chemistry research, yielding unusual mechanisms that can be exploited in catalysis. See, e.g., J. Cheng, X. Liu, J.A. Kattirtzi, J. VondeVondele and M. Sprik, Aligning Electronic and Protonic Energy Levels of Proton-Coupled Electron Transfer in Water Oxidation on Aqueous TiO₂. *Angewandte Chem. Int. Ed.* 2014, **53**, 12046-12050.
- ²⁸ A.W. Knight, P. Ilani-Kashkouli, J.A. Harvey, J.A. Greathouse, T.A. Ho, N. Kabengi and A.G. Ilgen *Environmental Science: Nano* 2020, **7**, 68-80.
- ²⁹ J.P. Perdew, K. Burke, and M. Ernzerhof, *Phys. Rev. Lett.* 1996, **77**, 3865-3868.
- ³⁰ G. Kresse, and J. Furthmüller, *Phys. Rev. B* 1996, **54**, 11169-11186.
- ³¹ G. Kresse, J. Furthmüller, *Comput. Mater. Sci.* 1996, **6**, 15-50.
- ³² G. Kresse and D. Joubert, *Phys. Rev. B* 1999, **59**, 1758-1775.
- ³³ J. Paier, M. Marsman and G. Kresse, *J. Chem. Phys.* 2007, **127**, 024103.
- ³⁴ K. Leung, I.M.B. Nielsen and L.J. Criscenti, *J. Am. Chem. Soc.*, 2009, **131**, 18358-18365.
- ³⁵ K. Leung, L.J. Criscenti, *J. Phys. Condens. Matter* 2012, **24**, 124015.
- ³⁶ S.L. Dudarev, G.A. Botton, S.Y. Savrasov, C.J. Humphreys and A.P. Sutton. *Phys. Rev. B*, 1998, **57**, 1505.
- ³⁷ Heyd, J.; Scuseria, G.E.; Ernzerhof, M. Hybrid Functionals based on a Screened Coulomb Potential. *J. Chem. Phys.* **2003**, *118*, 8207-8215.
- ³⁸ Heyd, J.; Scuseria, G.E.; Ernzerhof, M. Hybrid Functionals Based on a Screened Coulomb Potential. *J. Chem. Phys.* **2006**, *124*, 219906.
- ³⁹ Vydrov, O.A.; Heyd, J.; Krukau, A.V.; Scuseria, G.E. Importance of Short-Range versus Long-Range Hartree Fock Exchange for the Performance of Hybrid Density Functionals. *J. Chem. Phys.*, **2006**, *125*, 074106.
- ⁴⁰ M.G. Martin and A.P. Thompson, *Fluid Phase Equil.* 2004, **217**, 105-110.
- ⁴¹ H.J.C. Berendsen, J.R. Grigera and T.P. Straatsma, *J. Phys. Chem.* 1987, **91**, 6269-6271.
- ⁴² K. Leung, S.B. Rempe, C.D. Lorenz, *Phys. Rev. Lett.* 2006, **96**, 095504.
- ⁴³ See, e.g., S. Grimme, *J. Comput. Chem.*, 2006, **27**, 1787-1799.
- ⁴⁴ See, e.g., C. Zhang, J. Wu, G. Galli and F. Gygi, *J. Chem. Theor. Comput.*, 2011, **7**, 3054-3061.
- ⁴⁵ M. Pfeiffer-Laplaud, M.P. Gageot and M. Sulpizi, *J. Phys Chem. Lett.* 2016, **7**, 3229-3234.
- ⁴⁶ Y.R. Shen and V. Ostroverkhov. *Chem. Rev.* 2006, **106**, 1140-1154.
- ⁴⁷ A.M. Darlington and J. Gibbs-Davis *J. Phys. Chem. C* 2015, **119**, 16560-16567.

- ⁴⁸ C. Zhang, X. Liu, X. Lu, M. He, E.J. Meijer and R. Wang, *Geochim. Cosmochim. Acta* 2017, **203**, 54-68.
- ⁴⁹ L.E. Katz, L.J. Criscenti, C.-C. Chen, J.P. Larentzos and H.M. Liljestrand, *J. Coll. Interface Sci.* 2013, **399**, 68-76.
- ⁵⁰ J. Blumberger and M.L. Klein, *Chem. Phys. Lett.* 2006, **422**, 210-217.
- ⁵¹ S. Kerisit, S.P. Zarzycki and K.M. Rosso, *J. Phys. Chem. C* 2015, **119**, 9242-9252.
- ⁵² A. Laio and M. Parrinello, *M. Proc. Natl. Acad. Sci. USA* 2002, **99**, 12562-12566.
- ⁵³ N.R. Haria and C.D. Lorenz, *J. Phys. Chem. C* 2015, **119**, 12298-12311.
- ⁵⁴ N. Marzari and D. Vanderbilt, *Phys. Rev. B* 1997, **56**, 12847.
- ⁵⁵ D.A. Anderson, S.I. Simak, B. Johansson, I.A. Abrikosov and N.V. Skorodumova, *Phys. Rev. B* 2007, **75**, 035109.
- ⁵⁶ M. Nolan, S. Grigoleit, D.C. Sayle, S.C. Parker and G.W. Watson, *Sur. Sci.* 2005, **576**, 217-229.
- ⁵⁷ S. Lutfalla, V. Shapovadov and A.T. Bell, *J. Chem. Theoy Comput.* 2011, **7**, 2218-2223.
- ⁵⁸ D.J. Vogel, D.F. Sava Gallis, T.M. Nenoff and J.M. Rimsza, *Phys. Chem. Chem. Phys.* 2019, **21**, 23085.
- ⁵⁹ W. Piasecki and D.A. Sverjensky, *Geochim. Cosmochim. Acta* 2008, **72**, 3964-3979.
- ⁶⁰ T.R. Graham, M. Dembowski, E. Martinez-Baez, X. Zhang, *et al.*, *Inorg. Chem.* 2018, **57**, 11864-11873.
- ⁶¹ K. Leung and S.B. Rempe, *J. Am. Soc. Chem.* 2004, **126**, 344.